ISSN (Print) 1226-1750
ISSN (Online) 2233-6656
**Journal of Magnetics** 27(3), 272-277 (2022) https://doi.org/10.4283/JMAG.2022.27.3.272

# Calculation of Iron Loss with Stress in Stator Core by Shrinkage Tolerance

**Jung-Hyung Park, Hyungwon Shim, Yun-Ho Kim, and So-Young Sung***

*Alternative Fuels and Power System Research Division, Korea Research Institute of Ships & Ocean Engineering, Daejeon 34103, Republic of Korea*

(Received 28 April 2022, Received in final form 12 July 2022, Accepted 12 July 2022)

**This paper presents a method for calculating the iron loss of the stator core of an electric motor owing to the stress generated by shrink fit tolerance in the production process. Shrink fit is used to fix the frame and stator core, shaft, and rotor core in a motor, and the corresponding condition varies depending on the material. Three finite element analysis steps were performed to reduce the iron loss owing to stress during shrinking of a frame and stator core. In step 1, the shrink fit process was applied to a frame and stator core, considering the manufacturing tolerances through three-dimensional modeling. Thermal-structure finite element analysis was performed to apply the same conditions as those in the shrink fit process. The shrink fit was expanded by applying heat to the frame, followed by natural cooling to calculate the contact stress between the frame and the stator core. In step 2, the same contact stress as that in step 1 was derived using structural analysis through two-dimensional modeling of the frame and stator core without tolerances. The contact stress was calculated by applying the equivalent thermal expansion coefficient of the frame, and it was confirmed that the manufacturing tolerance and maximum stress intensity are linearly related. In step 3, electromagnetic analysis was performed at the rated operating point of the 2.2-kW induction motor using the model obtained in step 2. The magnetic flux density distribution of the stator core was derived via electromagnetic analysis and the iron loss, including the stress distribution, realized in step 2. The iron losses obtained under different conditions, including the stress of the stator core owing to the shrink fit tolerance, were compared, and the effectiveness of the shrink fit tolerance required to achieve a motor with high efficiency was evaluated.**

**Keywords :** stator core, shrink fit, tolerance, stress, iron loss

## 1. Introduction

Recently, improvements in the energy efficiency of electric machines have become a global concern, and the reliability of analyses related to electromagnetic loss has increased. The losses of an induction motor are classified into five categories based on the loss separation test (IEC60034-2-1): primary copper loss in the stator winding, secondary copper loss in the rotor conductor bar and rotor end ring, iron loss in the stator and rotor cores due to hysteresis and eddy currents, respectively, friction loss due to bearing friction or rotor vibration, and windage loss due to fluid flow, all of which are categorized as stray load losses [1, 2].

Iron losses in the stator core are induced by wire cutting, punching, and laser cutting, and hence are common in the cutting of electrical steel sheets, welding, interlocking, and self-bonding, which is a lamination method. Moreover, the iron loss depends on the cutting and lamination methods employed because the magnetic properties change depending on the stress applied to the electric steel sheet according to the manufacturing process [3-6]. In addition, it is known that the electrical properties of an electric steel sheet depend on the heat treatment conditions, and the stress decreases after heat treatment [7, 8]. The shrink fit of a motor involves the application of heat, and the electromagnetic loss depends on stress, which in turn depends on the manufacturing tolerances. The stress and iron loss due to shrink fit tolerance determine the efficiency of a motor; therefore, research is needed on this aspect.

This paper presents a method for calculating the iron loss of the stator core of induction motors owing to the stress generated by shrink fit tolerance in the production process. There are two types of shrink fit for an induction motor: one is used to fix the frame and stator core, and


*Corresponding author: Tel: +82-42-866-3853
Fax: +82-42-866-3862, e-mail: riverblu@kriso.re.kr

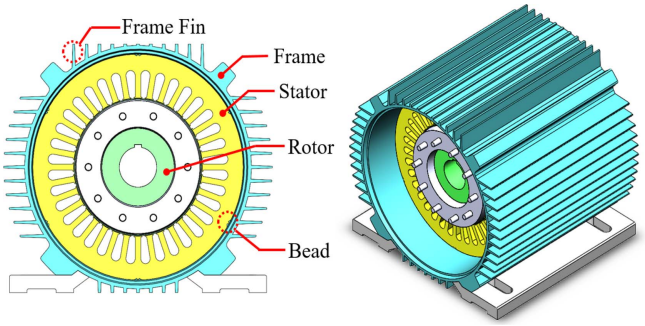


**Fig. 1.** (Color online) Shrink fit 3-D modeling of 2.2-kW induction motor.

the other is used to fix the shaft and rotor core.

Generally, the frame of an induction motor constitutes cast iron or aluminum, while the shaft is made of special-purpose steel. In this study, the stress and iron loss due to the shrink fit tolerance of a stator core were calculated v finite element analysis (FEA) in three steps. In step 1, the same analysis as the shrink fit process was performed through 3D modeling of the frame and stator core, considering four types of manufacturing tolerances, as shown in Fig. 1. The contact stress of each model was obtained following natural cooling of the stator core, after expansion, owing to the application of heat to the frame. In step 2, the stress distribution obtained in step 1 was derived using the equivalent coefficient of thermal expansion (ECTE) through a 2D model without tolerance. In step 3, the magnetic flux density distribution of the stator core was derived through electromagnetic analysis at the rated operating point of the 2.2-kW induction motor, and the iron loss including the stress was calculated by applying the stress distribution obtained in step 2. Finally, the validity of the iron-loss calculation, including the stress of the stator core against the shrink fit tolerance, was determined.

## 2. Shrink Fit Theory and Tolerance Modeling

### 2.1. Contact Stress

Shrink fit is a widely used assembly method to fix a stator to the frame or to constrain the axis of a rotor for rotation. More specifically, it is a restraining method that uses materials with different temperatures. In this method, the contact force $p$ between two materials is determined by the amount of interference, as follows [9]:

$$p = \frac{\Delta r}{\frac{r}{E_o}\left(\frac{r_o^2 + r^2}{r_o^2 - r^2} + v_o\right) + \frac{r}{E_i}\left(\frac{r_o^2 + r_i^2}{r_o^2 - r_i^2} + v_i\right)}, \quad (1)$$

where $v_o$ and $v_i$ are the Poisson's ratios of the stator core and the frame, respectively; $E_o$ and $E_i$ are the Young's moduli of the stator core and the frame, respectively; $r_o$ is the outer diameter of the stator core; $r_i$ is the inner diameter of the frame; $r$ is the inner diameter of the frame after fitting the stator core and the frame, and $\Delta r$ is the amount of interference.

### 2.2. Motor Modeling

A 2.2-kW induction motor was modeled with four poles and 36 slots. Considering a frame standard of 100 L, the outer diameter of the stator core and inner diameter of the frame were 180 mm. The minimum and maximum dimensional tolerances are –0.03 and 0 mm for the stator core, and –0.08 and –0.06 mm, for the frame. Four interference fits (maximum and minimum values of –0.03 and –0.08 mm, respectively) are generated from combining these dimensional tolerances. The stator core had four beads stacked through welding. The rotor core was skewed and the bar was made of aluminum.

The frame and rotor bars are made of aluminum alloy A1070 and have the following parameters: Young's modulus of 70 GPa, Poisson's ratio of 0.3, thermal conductivity of 230 W/m·°C, specific heat of 900 J/kg·°C, and CTE of $2.3 \times 10^{-5}$ m/m·°C. The stator and rotor cores are made of 50PN470, which are electric steel sheets with the Young's modulus of 200 GPa and Poisson's ratio of 0.3.

## 3. Coupled Analysis Procedure with Shrink Fit Tolerance

### 3.1. Shrink Process Analysis

The overall coupled analysis procedure is illustrated in Fig. 2. First, modeling was performed with four types of

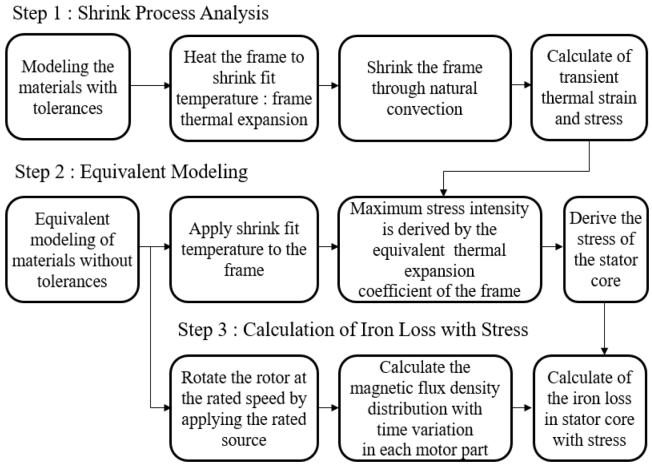


**Fig. 2.** Coupled analysis procedure of iron loss with shrink fit tolerance.

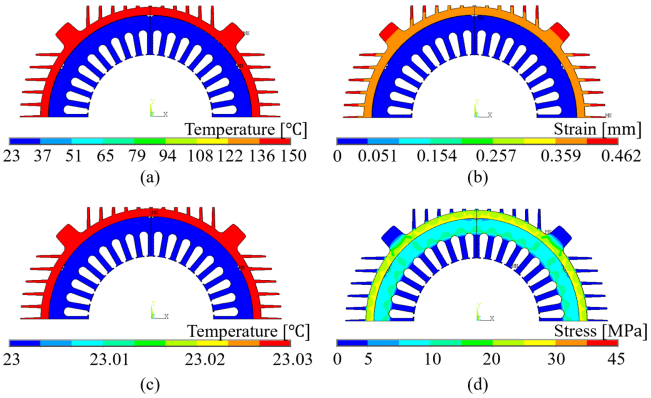


**Fig. 3.** (Color online) Results of step 1 (interference: −0.08 mm): (a) frame heating; (b) strain due to frame heating; (c) temperature after shrink fit; (d) stress after shrink fit.

interference owing to the tolerance between the stator core and the frame. The model with the amount of interference was applied to the frame at 150 °C using a heat transfer analysis at room temperature (23 °C). The frame was thermally expanded under structural symmetry conditions, and transient thermal strain and stress analyses under natural convection conditions were performed using the time-history method. After the shrink fitting process, the surface temperature inside and outside the stator was 23 °C, and the thermal conductivity coefficient of 10 W/m$^2$ °C was applied.

Fig. 3 presents the analysis results obtained under the same conditions as those used in the shrink fit process by modeling the interference amount of −0.08 mm. When the frame has the inner diameter tolerance of −0.08 mm and the stator core has the outer diameter tolerance of 0 mm, the magnitude of interference was observed to be the maximum value among the four models. Fig. 3(a) shows that the temperature of the frame was heated to 150 °C for a shrink fit. Consequently, the thermal clearance of the frame was 0.462 mm, as shown in Fig. 3(b). Figs. 3(c) and 3(d) present the temperature and contact stress, respectively, after shrink fitting.

Table 1 shows the stress intensity owing to the maximum contact pressure in the shrink fit state according to the dimensional tolerances of the stator core and frame. The maximum stress intensities after the shrink fit in the frame with the maximum and minimum interference amounts was 45 and 16.9 MPa, respectively. After shrink fitting, stress was constantly applied between the stator core and frame.

### 3.2. Equivalent Modeling

In step 1, it was confirmed that the stress increased as the shrink fit interference increased. On the one hand, there is the disadvantage that a new modeling procedure is required to determine the stress distribution for shrink fit tolerance. However, equivalent modeling is a general analysis model without shrink fit tolerance between the stator core and frame. The shrinkage of the equivalent model was determined using the CTE of the frame material. Therefore, the shrink fit of the equivalent modeling can be used to calculate the stress with tolerance using the ECTE, as:

$$\alpha_e = c_i x_i + \alpha_0 , \tag{2}$$

where $\alpha_e$ is the ECTE, $x_i$ is the amount of interference between the stator core and the frame, $c_i$ is the coefficient of interference, and $\alpha_0$ represents the CTE of the frame material. Using the ECTE, the stress with tolerance is given by:

$$p_i = \left(\frac{p_0}{\alpha_0}\right)\alpha_e , \tag{3}$$

where $p_i$ is the stress to which tolerance is applied after shrink fitting, and $p_0$ represents the stress to which tolerance is not applied after shrink fitting. The CTE and stress are linearly related. When using the ECTE, the temperature applied to the frame should be the same; the shrink fit temperature of 150 °C was applied in this study.

The stress distribution of the equivalent model without tolerance owing to ECTE is depicted in Fig. 4. The stress distribution of the stator core owing to the shrink fit appears mainly in the yoke. Table 2 lists the results of the stress intensity of the equivalent model owing to the equivalent coefficient of thermal expansion. From the

**Table 1.** Stress intensity due to interference in shrink fit condition.

| Stator core | | Frame | | Interference [mm] | Maximum Stress intensity [MPa] |
|---|---|---|---|---|---|
| Diameter [mm] | Tolerance [mm] | Diameter [mm] | Tolerance [mm] | | |
| 179.97 | −0.03 | 179.94 | −0.06 | −0.03 | 16.9 |
| 179.97 | −0.03 | 179.92 | −0.08 | −0.05 | 28.1 |
| 180 | 0 | 179.94 | −0.06 | −0.06 | 33.9 |
| 180 | 0 | 179.92 | −0.08 | −0.08 | 45.0 |

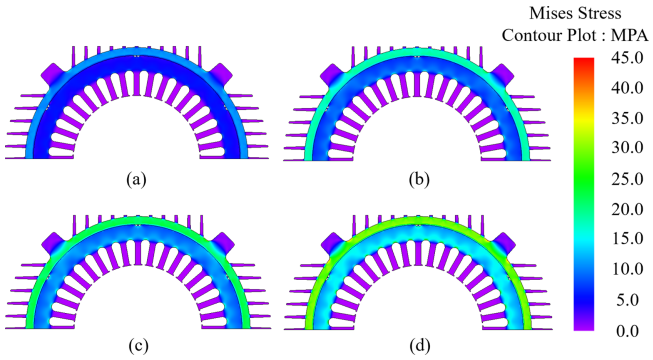


**Fig. 4.** (Color online) Stress distribution in the equivalent model without tolerance: (a) –0.03 mm; (b) –0.05 mm; (c) –0.06 mm; (d) –0.08 mm.

**Table 2.** Stress intensity of the equivalent model due to the equivalent coefficient of the thermal expansion.

| Step 1: Maximum Stress intensity [MPa] | ECTE [1/°C] | Maximum Stress intensity [MPa] | |
|---|---|---|---|
| | | Frame | Stator Core |
| 16.9 | 1.42e-06 | 16.9 | 12.1 |
| 28.1 | 2.35e-06 | 28.2 | 20.2 |
| 33.9 | 2.84e-06 | 33.8 | 24.3 |
| 45.0 | 3.77e-06 | 45.1 | 35.1 |

table, it can be observed that the error rate between the maximum stress intensity in step 1 and the maximum stress intensity by the ECTE is 0.07 % on average. The maximum stress intensity of the stator core was 36.7 % lower than the maximum stress intensity of the frame.

The stress distribution of the stator core was used to calculate the iron loss in step 3.

### 3.3. Calculation of iron loss with stress

Magnetic property data are required to calculate the iron loss of a stator core with stress [10-12]. Fig. 5 shows the magnetization and iron loss curves with the stress of 50PN470, which is frequently used in industrial induction motors. The original curve indicates the measured data of the commonly used industrial 50PN470, while the stress curve was obtained from the data provided by the electromagnetic field analysis software (JMAG). The stress was measured in the range of 25-100 MPa, and it was confirmed that the magnetic properties changed according to the stress. The magnetization curve tends to have a lower magnetic permeability and a smaller maximum magnetic flux density when the magnetic field strength is less than 1,000 A/m. The iron loss curve tended to increase the iron loss per magnetic flux density as the stress increased at the frequency of 60 Hz. The iron loss

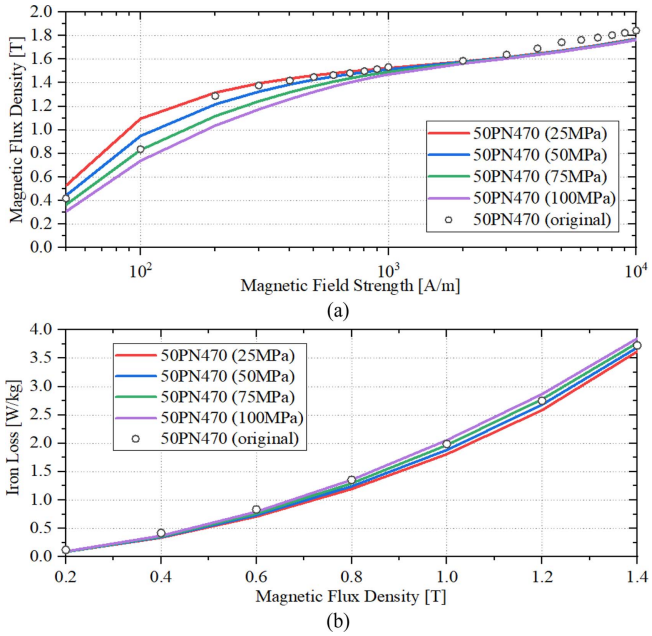


**Fig. 5.** (Color online) (a) Magnetization and (b) iron loss curves at 60 Hz of 50PN470.

of commercial motors is between 50 and 75 MPa and is expected to increase when the stress is greater than 75 MPa.

The magnetic flux density of the induction motor was obtained using 2D FEA of the equivalent model [13, 14]. The rated output of the induction motor was 2.2 kW, a commercial 220-V and 60-Hz source was used, and the rated speed was 1,767 rpm. Fig. 6(a) presents the distribution of the magnetic flux density of the stator core under the rated load condition. From the figure, it can be observed that the magnetic flux density tended to increase slightly around the beads. The maximum magnetic flux densities of the yoke and teeth in the stator core are 1.57 and 1.51 T, respectively. Fig. 6(b) shows the distribution of iron loss without stress in the equivalent model. The iron loss of the stator core without the stress component was calculated as 52.07 W, and the hysteresis and eddy current losses were found to be 25.25 and 26.82 W,

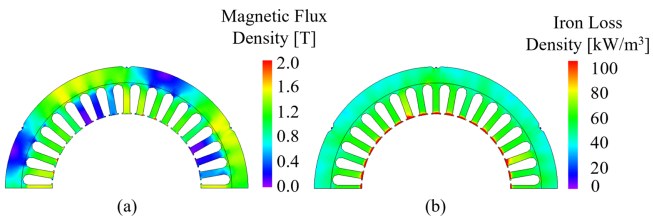


**Fig. 6.** (Color online) Analysis results without the stress of the equivalent model: (a) magnetic flux density distribution; (b) iron loss distribution.

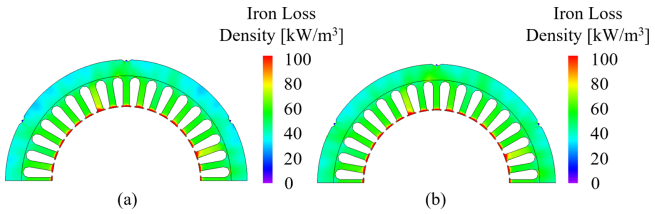


**Fig. 7.** (Color online) Iron loss distribution with stress of the equivalent model at (a) 0.08 mm and (b) 0.26 mm.

**Table 3.** Result of hysteresis loss and eddy current loss due to interference.

| Interference [mm] | Step 2: Maximum Stress intensity [MPa] | | Hysteresis loss [W] | Eddy current loss [W] |
|---|---|---|---|---|
| | Frame | Stator Core | | |
| 0.08 | 45.1 | 32.4 | 26.409 | 24.972 |
| 0.14 | 78.9 | 56.7 | 26.541 | 25.408 |
| 0.20 | 112.7 | 81.0 | 26.315 | 26.287 |
| 0.26 | 146.5 | 105.3 | 26.293 | 26.832 |

respectively.

Figs. 7(a) and 7(b) display the distributions of iron loss in the stator core with maximum stress intensities of 32.4 and 105.3 MPa, respectively. Table 3 lists the calculation results of the iron loss due to interference. As the interference increased, the eddy current loss among the iron loss components tended to increase. The commercial steel sheet has a value between 56.7 and 81.0 MPa, and no increase in the iron loss is expected for a shrink fit tolerance of 0.2 mm. Fig. 8 indicates a linear relationship between the ECTE and the maximum stress intensity owing to interference. Fig. 9 shows the iron loss due to interference; the trend line was calculated using a quadratic polynomial, and the R-squared values of the hysteresis loss and eddy current loss were determined as 0.6034 and 0.9846, respectively. From the figure, it can be seen that the commercial steel sheets have the same iron loss at 0.15-mm interference, and the interference at 0.4 mm increases the iron loss by 4.23 % compared with that of the commercial steel sheets, corresponding to the increase of 0.1 % in the efficiency of the 2.2-kW induction motor.

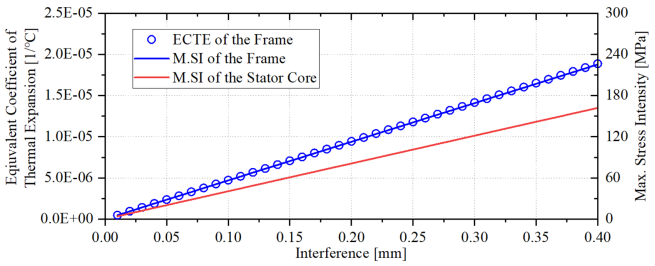


**Fig. 8.** (Color online) ECTE and maximum stress intensity as a function of interference.

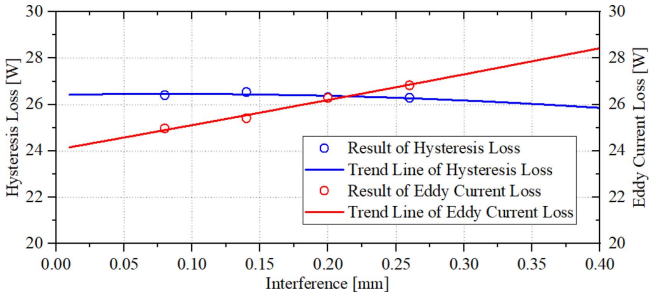


**Fig. 9.** (Color online) Iron loss as a function of interference.

## 4. Conclusion

In this study, the iron loss owing to the stress of the stator core with shrink fit tolerance was calculated. Through a three-step FEA, the relationship between interference and iron loss was derived. In step 1, the shrink fit process was analyzed using a 3D model with tolerances to derive the stress. In step 2, the stress obtained in step 1 was derived using the ECTE through a 2D equivalent model without tolerances. In Step 3, a magnetic field density analysis was performed at the rated operating point of the equivalent model to derive the magnetic flux density distribution, and the iron loss was calculated by applying the stress data of the electric steel sheet.

From the analysis results, a linear relationship was observed between the interference and effective value of manufacturing tolerance from the contribution of efficiency to iron loss.

## Acknowledgement

This research was supported by a grant from “Development on operation and reliability verification technology of 1 MW class eco-friendly ship fuel and power system under ocean environment” Program funded by Ministry of Oceans and Fisheries of Korean government (1525012259/PMS5020). This work was also supported by a “Development of basic technologies in eco-friendly ship fuel reliability and safety evaluation” Program funded by Korea Research Institute of Ships & Ocean Engineering (PES4301).

## References

[1] Y. Gao et al., IEEE Trans. Magn. **49**, 5 (2013).
[2] A. Cavagnino, S. Vaschetto, L. Ferraris, Z. Gmyrek, E. B. Agamloh, and G. Bramerdorfer, IEEE Trans. Ind. **56**, 1 (2020).

[3] R. Siebert, J. Schneider, and E. Beyer, IEEE Trans. Magn. **50**, 4 (2014).
[4] T. P. Holopainen, P. Rasilo, and A. Arkkio, IEEE Trans. Ind. **53**, 2 (2017).
[5] M. Bali, H. De Gersem, and A. Muetze, IEEE Trans. Ind. **53**, 5 (2017).
[6] H. A. Weiss, P. Tröber, R. Golle, S. Steentjes, N. Leuning, S. Elfgen, K. Hameyer, and W. Volk, IEEE Trans. Ind. **54**, 6 (2018).
[7] T. Kinoshita, K. Kohara, H. Shimoji, T. Sato, and T. Todaka, IEEE Trans. Magn. **54**, 11 (2018).
[8] T. Kinoshita, H. Shimoji, S. Aihara, T. Sato, and T. Todaka, IEEE Trans. Magn. **55**, 2 (2019).
[9] S. P. Timoshenko, Strength of Material: Part 2: Advanced Theory and Problems 3rd edition. Van Nostrand, London (1956) pp 208-214.
[10] K. Yamazaki and W. Fukushima, IEEE Trans. Magn. **51**, 3 (2015).
[11] K. Yamazaki, Y. Sato, M. Domenjoud, and L. Daniel, IEEE Trans. Magn. **56**, 3 (2020).
[12] H. Zhang, L. Zeng, D. An, and R. Pei, IEEE Trans. Magn. **58**, 2 (2022).
[13] K. Yamazaki and Y. Kato, IEEE Trans. Magn. **50**, 2 (2014).
[14] M. Aminu, P. Barendse, and A. Khan, IEEE Trans. Ind. **67**, 9 (2020).